AGU PUBLICATIONS

JGR

Journal of Geophysical Research: Oceans

RESEARCH ARTICLE

10.1002/2015JC011283

Special Section:
Forum for Arctic Modeling and Observing Synthesis (FAMOS): Results and Synthesis of Coordinated Experiments

Short-term sea ice forecasting: An assessment of ice concentration and ice drift forecasts using the U.S. Navy's Arctic Cap Nowcast/Forecast System

David A. Hebert[1], Richard A. Allard[1], E. Joseph Metzger[1], Pamela G. Posey[1], Ruth H. Preller[1], Alan J. Wallcraft[1], Michael W. Phelps[2], and Ole Martin Smedstad[3]

[1]Naval Research Laboratory, Stennis Space Center, Mississippi, USA, [2]Jacobs Technology Inc., Stennis Space Center, Mississippi, USA, [3]Vencore Services and Solutions, Inc., Stennis Space Center, Mississippi, USA

Key Points:
- Five day ice concentration forecast skill, ice edge prediction and ice motion compared to observations
- Improve forecasts by assimilating National Ice Center IMS into U.S. Navy sea ice forecast system
- Skill of U.S. Navy ice forecasting compared to persistence and climatology

Correspondence to:
D. Hebert,
david.hebert@nrlssc.navy.mil

Citation:
Hebert, D. A., R. A. Allard, E. J. Metzger, P. G. Posey, R. H. Preller, A. J. Wallcraft, M. W. Phelps, and O. M. Smedstad (2015), Short-term sea ice forecasting: An assessment of ice concentration and ice drift forecasts using the U.S. Navy's Arctic Cap Nowcast/Forecast System, *J. Geophys. Res. Oceans*, *120*, doi:10.1002/2015JC011283.

Received 1 SEP 2015
Accepted 19 NOV 2015
Accepted article online 23 NOV 2015

Abstract In this study the forecast skill of the U.S. Navy operational Arctic sea ice forecast system, the Arctic Cap Nowcast/Forecast System (ACNFS), is presented for the period February 2014 to June 2015. ACNFS is designed to provide short term, 1–7 day forecasts of Arctic sea ice and ocean conditions. Many quantities are forecast by ACNFS; the most commonly used include ice concentration, ice thickness, ice velocity, sea surface temperature, sea surface salinity, and sea surface velocities. Ice concentration forecast skill is compared to a persistent ice state and historical sea ice climatology. Skill scores are focused on areas where ice concentration changes by ±5% or more, and are therefore limited to primarily the marginal ice zone. We demonstrate that ACNFS forecasts are skilful compared to assuming a persistent ice state, especially beyond 24 h. ACNFS is also shown to be particularly skilful compared to a climatologic state for forecasts up to 102 h. Modeled ice drift velocity is compared to observed buoy data from the International Arctic Buoy Programme. A seasonal bias is shown where ACNFS is slower than IABP velocity in the summer months and faster in the winter months. In February 2015, ACNFS began to assimilate a blended ice concentration derived from Advanced Microwave Scanning Radiometer 2 (AMSR2) and the Interactive Multisensor Snow and Ice Mapping System (IMS). Preliminary results show that assimilating AMSR2 blended with IMS improves the short-term forecast skill and ice edge location compared to the independently derived National Ice Center Ice Edge product.

1. Introduction

Recent satellite observations have shown that the Arctic September sea ice extent minimum has been decreasing at a more rapid rate in the past two decades (1997–2014) than the first two decades when satellite observations were first made in 1979 [*Serreze and Stroeve*, 2015, Figure 2]. This increased rate of decline in sea ice cover means a greater area of navigable waters in the Arctic will be available for longer periods of time. The ability to forecast ice conditions is of crucial importance for maritime operational planning [*U.S. Navy*, 2014] and for scientific applications such as monitoring oceanographic [*Johannessen et al*., 2004; *Serreze et al*., 2007] and biologic [*Arrigo et al*., 2008; *Aschan and Ingvaldsen*, 2009; *Durner et al*., 2011; *Jay et al*., 2011] conditions. The Naval Research Laboratory (NRL) has a long history of Arctic forecast systems, going back to 1987 with the Polar Ice Prediction System (PIPS) [*Preller et al*., 2002], an Arctic basin forecast system consisting of the *Hibler* ice model [*Hibler*, 1979, 1980] and a monthly mean ocean climatological forcing. This system was replaced by PIPS 2.0, a 25 km resolution system coupling the Hibler ice model to the Cox ocean model [*Cox*, 1984] and encompassed all the sea ice covered regions of the northern hemisphere. With many recent improvements in sea ice and ocean modeling, as well as advances in high performance computing, the next generation Arctic forecast system, the Arctic Cap Nowcast/Forecast System (ACNFS), has been developed. ACNFS uses the Los Alamos Community Ice CodE (CICE) version 4.0 [*Hunke and Lipscomb*, 2008] as the sea ice model which is two-way coupled to the HYbrid Coordinate Ocean Model (HYCOM) [*Bleck*, 2002; *Metzger et al*., 2014, 2015].

There are many ice-ocean modeling systems currently in use. The Community Earth System Model (CESM) [*Kay et al*., 2015] is a global, fully coupled atmospheric-ice-ocean model and is freely available at https://www2.cesm.ucar.edu/models/current. The Estimating Circulation and Climate of the Ocean (ECCO) project

is a global ice-ocean state estimation using an adjoint method [*Stammer et al.*, 2002; *Wunsch and Heimbach*, 2013]. The Canadian Global Ice Ocean Prediction System (GIOPS) [*Smith et al.*, 2015] provides a daily global ice and ocean analysis and 10 day forecasts using CICE coupled to the eddy-permitting, 1/4° Nucleus for European Modeling of the Ocean (NEMO). Several regional ice-ocean models are also published. Full Arctic domain models include the Pan Arctic Ice Ocean Modeling and Assimilation System (PIOMAS) [*Schweiger et al.*, 2011; *Zhang and Rothrock*, 2003], a recent evolution of PIOMAS called Marginal Ice Zone Modeling and Assimilation System (MIZMAS), [*Schweiger and Zhang*, 2015], the Naval Postgraduate School Arctic Modeling Effort (NAME) [*Maslowski et al.*, 2004; *McGeehan and Maslowski*, 2012], and the TOPAZ System [*Bertino and Lisæter*, 2008; *Sakov et al.*, 2012]. Smaller sub-arctic regions include the Canadian Regional Ice Prediction System (RIPS) [*Buehner et al.*, 2013; *Lemieux et al.*, 2015], the Nares Strait [*Rasmussen et al.*, 2010], and Labrador Sea and Baffin Bay [*Fenty and Heimbach*, 2013]. Finite element [*Scholz et al.*, 2013; *van Scheltinga et al.*, 2010] and finite volume [*Gao et al.*, 2011] ice models also have been used to study ice-ocean dynamics. With the exception of the Canadian RIPS, MIZMAS, and TOPAZ, these models are used for either hindcasts (predictions of past events) or multi-decadal climate studies. ACNFS, in contrast, is designed to produce short-term, 1-7 day forecasts of current ice conditions with a focus on the marginal ice zone where ships are most likely to travel.

The aim of this paper is to document ACNFS and validate sea ice forecasts up to 5 days. A detailed description of the model is presented in section 2, followed by the forecast assessments and results in section 3. A summary is provided in section 4.

2. The Arctic Cap Nowcast/Forecast System (ACNFS)

ACNFS is a data assimilative, two-way coupled sea ice – ocean model driven by external atmospheric forcing. ACNFS [*Posey et al.*, 2010] was declared operational by the U.S. Navy in September 2013, and is run daily providing Arctic sea ice forecasts out to 7 days. A description of each model, coupling between models, forcing, and data assimilation are now presented.

2.1. Ice Model: CICE V4.0

The Los Alamos Community Ice Code (CICE) version 4.0 [*Hunke and Lipscomb*, 2008] is the ice component currently used in ACNFS. Within CICE, sea ice and snow are divided into several discrete ice thickness categories. In ACNFS there are five thickness categories; within each thickness category there are four ice layers and one snow layer (these settings are the CICE defaults). For each ice and snow layer, changes in thickness by thermodynamic processes including radiative, turbulent, and conductive heat fluxes are computed via an energy conserving thermodynamic model [*Bitz and Lipscomb*, 1999]. The model ice thickness distribution varies in time due to thermodynamic and mechanical processes (e.g., ridging), and is updated using the ice thickness remapping scheme of *Lipscomb* [2001]. Ice momentum is solved using the elastic-viscous-plastic (EVP) model [*Hunke and Dukowicz*, 1997, 2002]. EVP is a modification to traditional viscous-plastic (VP) models [e.g., *Hibler*, 1979] where elastic waves are allowed to exist in the ice. This modification allows the momentum equation to be computed with a much more efficient, fully explicit numerical scheme, as opposed to an implicit scheme used in VP models. The elastic waves, while nonphysical, are damped out by subcycling every time step. In ACNFS the time step is 10 min, with 120 subcycles per time step.

2.2. Ocean Model: HYCOM

The HYbrid Coordinate Ocean Model (HYCOM) [*Bleck*, 2002; *Chassignet et al.*, 2003] is the ocean model used in ACNFS. HYCOM combines three different vertical coordinates: (1) pressure (fixed depth), best in mixed layer and unstratified ocean, (2) sigma or terrain following, often the best choice in shallow water, and (3) isopycnal (density), with best application in the deep stratified ocean. There are 32 HYCOM vertical layers in ACNFS. While the number of total layers stays the same, it is possible for the number of each type of layer to change each time step. The model makes a dynamically smooth transition between coordinate types by using a layered continuity equation. The K-Profile Parameterization (KPP) [*Large et al.*, 1994] is used to parameterize vertical mixing.

2.3. Ice-Ocean Model Coupling

In ACNFS, CICE and HYCOM are two-way coupled via the Earth System Modeling Framework (ESMF) [*Campbell et al.*, 2010; *Hill et al.*, 2004]. CICE and HYCOM are run individually and exchange output every model hour. Table 1 contains a list of quantities coupled between each model. Ice thickness, fluxes, and

Table 1. Quantities Exchanged Between CICE and HYCOM Every Hour

From CICE to HYCOM	From HYCOM to CICE
Ice concentration	Sea surface temperature
Ice x/y stresses	Sea surface salinity
Heat flux through ice	Sea surface x/y velocities
Ice freeze/melt heat flux	
Net water flux	

stresses are sent to HYCOM from CICE while sea surface temperature, sea surface salinity, and sea surface currents are sent from HYCOM to CICE.

2.4. Atmospheric Forcing

The atmospheric forcing for ACNFS is currently provided by the NAVy Global Environment Model (NAVGEM) [*Hogan et al*., 2014]. (Prior to August 2013, forcing was provided by the Navy Operational Global Atmospheric Prediction System (NOGAPS) [*Hogan et al*., 1991]. NOGAPS was decommissioned in August 2013, with NAVGEM taking its place. Further details about the conversion from NOGAPS to NAVGEM are provided in *Metzger et al*. [2013].) NAVGEM is a spectral model with triangular truncation at wave number 425 (approximately 0.28 degree horizontal resolution). Output from NAVGEM is currently provided for use by ACNFS and other Navy applications on a uniformly spaced, 0.5 degree grid. (In the future, NAVGEM output is planned to be provided on its native 0.28 degree grid). NAVGEM provides output fields at 3 h intervals including 2 m air temperature, surface humidity, net surface shortwave and longwave radiation, precipitation, 10 m zonal and meridional wind velocities, mean sea level pressure, and 2 m dew point. These values are interpolated to the ACNFS computational grid for use in each daily run.

2.5. Data Assimilation

Observational data assimilation is achieved via the Navy Coupled Ocean Data Assimilation (NCODA) [*Cummings*, 2011; *Cummings and Smedstad*, 2013]. Data assimilation is performed to reduce errors in model forecasts due to several factors including nonlinear processes that are not a deterministic response to atmospheric forcing, poorly parameterized physical processes, limitations in numerical algorithms, and limitations due to model resolution. NCODA uses the 3-D variational analysis (3DVAR) method to assimilate observations into the model. Observational data that are assimilated into ACNFS come from a variety of sources. Most of the observed ocean surface data come from satellite-borne instruments. Sea surface height is obtained from Ocean Surface Topography Mission (OSTM)/Jason-2, AltiKa, and CryoSat-2. Sea surface temperature is obtained from the Advanced High Resolution Radiometer (AVHRR) (AVHRR methodology is the same as described in *Cayula et al*. [2013] for Visible Infrared Imaging Radiometer Suite (VIIRS)), Geostationary Operational Environmental Satellite (GOES), Meteosat Second Generation (MSG) satellite, and Advanced Microwave Scanning Radiometer 2 (AMSR2). Ice Concentration is obtained from the Defense Meteorological Satellite Program (DMSP) Special Sensor Microwave Imager/Sounder (SSMI/S) and AMSR2. Ice concentration from SSMI/S is derived using the NASA Team 2 sea ice algorithm [*Markus and Cavalieri*, 2000, 2009], while ice concentration from AMSR2 is derived from the Bootstrap Algorithm [*Comiso*, 1986; *Comiso and Nishio*, 2008]. While these observations are useful for correcting surface conditions, observations below the surface are also desired to help correct ocean quantities at depth. Observations below the surface that are assimilated into ACNFS include temperature and salinity profiles from expendable bathythermographs (XBT) and conductivity-temperature-depth (CTD) profiles. Ice-Tethered Profiler data [*Krishfield et al*., 2008; *Toole et al*., 2011] provide temperature and salinity profiles below the sea ice to depths of 760 meters, and are available in near real-time and assimilated into HYCOM. Sea surface height observations are converted to a synthetic vertical temperature and salinity profile via the Modular Ocean Data Assimilation System (MODAS) system [*Fox et al*., 2002]. Temperature observations are also obtained from profiling floats such as Argo (www.argo.net).

NCODA performs data assimilation in a two-step process. First, all observational data are quality controlled (QC'd) to ensure erroneous data are not assimilated. The QC process is detailed in *Cummings* [2005, 2011]. Briefly, a series of initial "sanity checks" are performed including a land-sea boundary test and valid physical data range tests, followed by instrumentation error checks, and then cross validation checks for consistency of observations. After these checks, the data are compared to "background" fields, which include climatology and short-term (past few weeks) observation analyses. A probability of error is then calculated based on the difference between the observation and background data. The sea ice concentration climatology is obtained from the European Centre for Medium Weather Forecast (ECMWF) climatology formed from years 1979 to 1996 [*Fernandez et al*., 1998], while ocean climatologies are obtained from Generalized Digital Environmental Model (GDEM) [*Carnes et al*., 2010]. If the observation probability of error reaches a specified

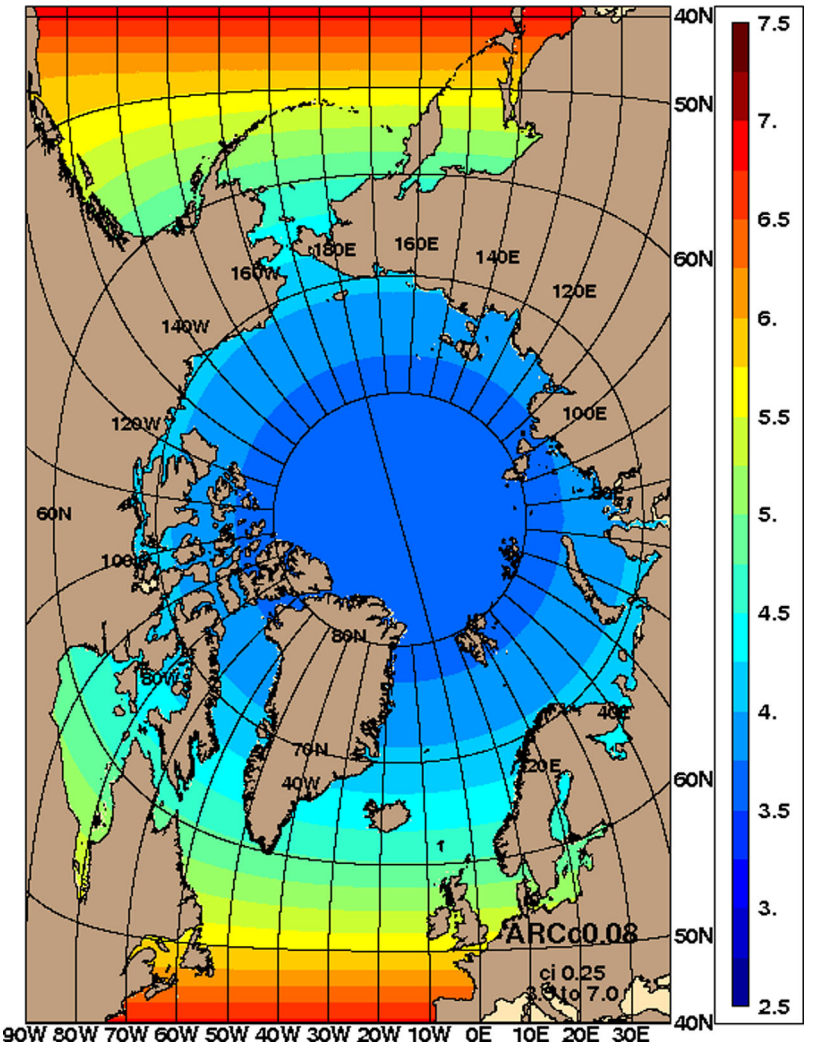

Figure 1. ACNFS horizontal grid spacing in km.

threshold (usually 5%), the data are not assimilated. Second, the QC'd data are then used in the 3DVAR method to create an analysis field based on the observed and background data and the error covariance. The NCODA ice and ocean analysis fields are then used for data assimilation into the model.

2.5.1. Assimilation With IMS

The Interactive Multisensor Snow and Ice Mapping System (IMS) [*Helfrich et al*., 2007] is an operational snow and ice mask product produced daily and valid at 00Z (Zulu, or Greenwich Mean Time). IMS is produced by an analyst at the National Ice Center (NIC) and incorporates a multitude of satellite imagery data including visible/infrared (VIS/IR), synthetic aperture radar (SAR), scatterometer, and passive microwave. The result is a sea ice extent mask that is available at either 1 km or 4 km spatial resolution. The IMS ice mask is available as a plain text file and GeoTiff [*NIC*, 2008]. (Note that IMS is also sent to the National Snow and Ice Data Center (NSIDC), repackaged into additional user-friendly formats such as Keyhole Markup Language (KML) and ESRI Shapefiles, and made available to the public as the Multisensor Analyzed Sea Ice Extent (MASIE) product [*Fetterer et al*., 2010].)

As discussed in *Posey et al*. [2015], the effective resolutions of observed sea ice concentration from SSMI/S and AMSR2 are 25 km and 10 km, respectively. These observed values must be interpolated to the higher resolution model grid (Figure 1). With model horizontal resolution 3.5 – 4.0 km north of 70°N, the relative coarseness of these data can lead to shifts in observed ice edge location compared to the model by 2–6 grid points, on the order of 10 km – 20 km. While the use of the IMS mask at 4 km resolution helps mitigate the observed versus model resolution differences, IMS is a product that can vary depending on the

availability of satellite coverage on a particular day. For example, SAR or VIS/IR observations are not available at all locations on all days. Also, IMS is a product created by human analysts, and subjective differences in ice location can occur [*Meier et al*., 2015].

The 4 km resolution IMS is used to mask the ice concentration assimilated into ACNFS, as 4 km is similar to the ACNFS horizontal resolution. IMS is a mask of ones and zeros that identify where the ice concentration is greater than 40%; there is no ice concentration value included within IMS. Since ACNFS requires a numeric ice concentration value for data assimilation, a method is required to convert the IMS mask to an ice concentration. Such a method was developed and described in *Posey et al*. [2015], where the IMS mask is applied to the NCODA analysis ice concentration, A, as follows:

$$A=\begin{cases} 0\%, & \text{IMS}=0 \\ 70\%, & \text{IMS}=1 \text{ and } A<70\% \\ A, & \text{IMS}=1 \text{ and } A\geq 70\% \end{cases} \quad (1)$$

In (1), if IMS = 0, the NCODA analysis ice concentration is removed and made 0%. If IMS = 1 and NCODA analysis ice concentration is less than 70%, NCODA analysis ice concentration is made to be 70%. If IMS = 1 and the NCODA analysis ice concentration is greater or equal to 70%, the NCODA analysis ice concentration value is not changed. The threshold of 70% was chosen as the midpoint of the range of valid IMS ice concentration values (40%–100%) [*Posey et al*., 2015]. This blending algorithm in (1) was created in conjunction with the NSIDC [*Fetterer et al*., 2015]. The difference is that *Fetterer et al*. [2015] apply (1) to AMSR2 ice concentration, whereas in ACNFS equation (1) is applied to the NCODA analysis ice concentration. The blending method of IMS and NCODA analysis ice concentration was first introduced to ACNFS 2 February 2015. This date is noted in the forecast assessments to investigate the effect of IMS on ACNFS forecasts.

2.5.2. Assimilating Sea Ice Concentration

Once the sea ice analysis field is created (blended with AMSR2 and IMS after February 2015), it is assimilated into ACNFS using the following algorithm:

1. If model < NCODA analysis
   a. Use NCODA analysis for model < 15%.
   b. Linearly blend model and NCODA analysis where (15% < model < 30%)
   c. Use model where model > 30%
2. If model ≥ NCODA analysis
   a. If NCODA < 1%, remove all ice.
   b. Otherwise:
      i. Use NCODA analysis where NCODA analysis < 25%
      ii. Linearly blend model and NCODA analysis where (25% < NCODA < 50%)
      iii. Use model where NCODA analysis > 50%

This assimilation method varies depending if the initial model ice concentration is less than or greater than the NCODA ice concentration. The algorithm is designed to assimilate near the ice edge, the area of most interest for U.S. Navy and other maritime operations. The main reasons for choosing this algorithm are twofold: first, it has been determined that sea ice obtained from SSMI/S using the Navy Cal-Val algorithm overestimates ice concentration in the central Arctic [*Hollinger*, 1991]; second, passive microwave sensors such as SSMI/S and AMSR2 tend to underestimate ice concentration in regions of thin ice or where meltponds exist on the sea ice surface [*Meier et al*., 2015]. The result is a weighted average of the NCODA sea ice analysis field and the modeled initial conditions. As seen in the algorithm, the threshold where ice is assimilated varies depending on whether the sea ice analysis field is greater or less than the model initial condition. In case 1 of the algorithm, the model ice concentration is less than NCODA, and thus ice needs to be added to the model. We only add ice in the vicinity of the modeled ice edge, where the model ice concentration is less than 30%. Where the model is less than 15%, NCODA is directly inserted into the model. Where the model is between 15% and 30%, a linear weighting is applied that puts more weight on the model value the closer it is to 30%. Above 30% the model value is retained. In case 2 of the algorithm, the modeled ice concentration is greater than NCODA, thus ice needs to be removed. Where the NCODA ice concentration

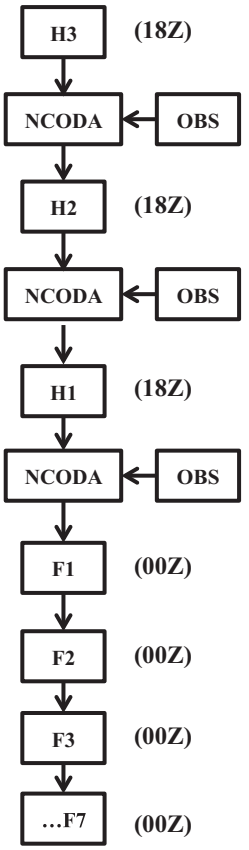

Figure 2. Flowchart of the hindcast/forecast process, where H=Hindcast, F=Forecast. The number indicates day of hindcast or forecast, so H3 = 3 day Hindcast, F1 = 1 day Forecast, etc. The number in parenthesis indicates the model hour. Thus, starting from H1, the first forecast time at 00Z is a 6 h forecast. The next forecast is the next day at 00Z, making it a 30 h forecast, etc.

is less than 25%, it is directly inserted into the model. Where NCODA is between 25% and 50%, a linear weighting is applied between the model and NCODA with more weight on the model as the NCODA value increases. Where NCODA is greater than 50% the model value is retained. In addition to the change in ice concentration, the modeled sea surface temperature is adjusted to be slightly above or below the freezing point, based on the addition or removal of ice, to prevent the model from immediately melting or forming sea ice based on sea surface temperature.

In regard to assimilating NCODA blended with IMS, we note that after blending the minimum NCODA ice concentration value (other than zero) is 70%. In the instance where the model ice concentration is less than 15% and IMS=1 (NCODA = 70% ice), a value of 70% is inserted into the model. Nearby there may be a model value of 30%, where the NCODA value is not assimilated and the 30% is retained. This could lead to regions with sharp gradients between 70% and 30%. In practice, this situation occurs rarely, as the region where ice changes from 15% to 30% is usually very narrow. Also, since this method is focused near the ice edge where the change is greatest, daily assimilation updates in the ice edge minimizes the long-term impact.

2.6. Model Setup

ACNFS has a horizontal resolution of 3.5–4.0 km in the polar latitudes north of 70°N (Figure 1). South of 70°N, the horizontal resolution gradually increases to 7.5 km at 40°N. At the open boundary at 40°N, in the Atlantic and Pacific Oceans, Neumann (reflective) boundary conditions are applied in CICE, while in HYCOM the boundary conditions are obtained from a real-time 1/12° global HYCOM/NCODA forecast system with an embedded thermodynamic sea ice model in place of CICE [*Metzger et al.*, 2008]. Neumann boundaries are used in CICE since 40°N is adequately far away from any sea ice covered region. HYCOM model bathymetry is based on the NRL 2 min Digital Bathymetric Database (DBDB2, http://www7320.nrlssc.navy.mil/DBDB2_www/).

Figure 2 contains a flowchart of how ACNFS is run each forecast period. For each 7 day forecast period, a 3 day hindcast is performed where ACNFS is first started 3 days prior to the current date. During this 3 day hindcast is when observational data are assimilated into the system. The reason for this is two-fold: (1) to assimilate data that may only be available 2 or 3 days after the observation time, and (2) to minimize the shock of replacing data in the model by starting back in time and gradually running to the assimilated value. After this 3 day hindcast, data are no longer available for assimilation, and a 7 day forecast is run. Note that the hindcasts are started at 18Z, while the forecasts are generated at 00Z. Thus, the first output from an 18Z start time is at 00Z the next day, making it a 6 h forecast. For the remainder of this paper forecast times will be referred to by hour (6 h, 30 h, etc.) instead of day (1 day, 2 days, etc.).

3. Forecast Assessments

3.1. Ice Concentration Forecast Skill

In assessing the ice concentration forecast skill of ACNFS, a skill score using the mean square error is computed based on the analysis of *Murphy and Epstein* [1989] and *Van Woert et al.* [2004]. Following the notation of *Van Woert et al.* [2004], skill score is generically defined as:

$$SS = \frac{\lambda_f - \lambda_R}{\lambda_p - \lambda_R} \tag{2}$$

where λ_f, λ_p, λ_R are the accuracy of the forecast, the accuracy of a "perfect" forecast, and the accuracy of a reference forecast, respectively. Accuracy is defined in terms of the mean-square error (MSE) [*Murphy and Epstein*, 1989], defined here as:

$$MSE(a,b) = \frac{1}{N}\sum_{i=1}^{N}(a_i - b_i)^2 \tag{3}$$

where a_i, b_i are values at location i, and N is the number of locations examined. (Selection of the i locations is described below.) Substitution of (3) into (2), and noting that MSE of a perfect forecast is zero (since $a=b$), yields:

$$SS = 1 - \frac{MSE(f,O)}{MSE(R,O)} \tag{4}$$

where f is the model forecast, O is an observed ice concentration, and R is a reference ice concentration used for comparison with the forecast. In (4), when the forecast MSE is less than the reference MSE, SS is positive and approaches 1. In contrast, if the forecast MSE is equal to or greater than the reference MSE, SS is zero or negative. Thus, $SS > 0$ indicates "skill" or improvement compared to reference field, whereas $SS \leq 0$ indicates no skill. In this paper two reference states are examined: climatology and persistence.

It is important to note that in (4), the observed field, O, in this study is the assimilated analysis field after the application of the assimilation algorithm described in section 2.5.2, and not the raw satellite ice concentration nor the raw NCODA analysis field. The reason for the use of the assimilated ice concentration for O is that the assimilation technique is designed to be our best estimate of the "true" ice coverage, particularly near the ice edge, given known biases in satellite ice concentration observations. Also, since the NCODA analysis field is modified by the weighting technique, the model never starts with an ice concentration that is the same as the observation field. Thus, using the raw observation would not be consistent with how the model is run.

The skill score relative to climatology is a measure of the skill of the model ice concentration forecast compared to assuming a climatological value. From (4), the climatology skill score is defined as

$$SS_c(n) = 1 - \frac{MSE(f_n, A_n)}{MSE(C_n, A_n)} \tag{5}$$

where n is the model forecast hour $n=(6, 30, 54, 78, 102, 126)$, f_n is the corresponding ice concentration forecast field, C_n is the ice concentration from the ECMWF ice concentration climatology, and A_n is the assimilated ice concentration obtained as in section 2.5.2. In (5), O is replaced by A_n seen in (4) to note the use of the assimilated ice concentration.

The skill score relative to persistence is a measure of model forecast ice concentration compared to assuming the conditions at the initial time will persist throughout the forecast period (i.e., conditions will stay the same). Here the skill score for persistence is defined as

$$SS_p(n) = 1 - \frac{MSE(f_n, A_n)}{MSE(A_0, A_n)} \tag{6}$$

where A_0 is the initial assimilated ice concentration (section 2.5.2) at the start of the forecast, and the other terms are as previously defined above.

In selecting the locations of interest, i, in (3), we are interested in the skill of ACNFS where the ice concentration changes. In this study, the locations were determined by identifying where the assimilated ice concentration changes by $\pm 5\%$ or more over 5 days. This is similar to the selection of points performed in *Lemieux et al*. [2015], and is simply the magnitude of the difference between the assimilated ice concentration at the start of the forecast and the assimilated ice concentration from the run started 5 days later. This method captures both ice formation and melt. Sample locations are shown in Figure 3 for March 2014 and September 2014, where it is seen that the points are located along the ice edge and marginal ice zone. It is important to note that the assimilation scheme described in section 2.5.2 only assimilates ice concentration

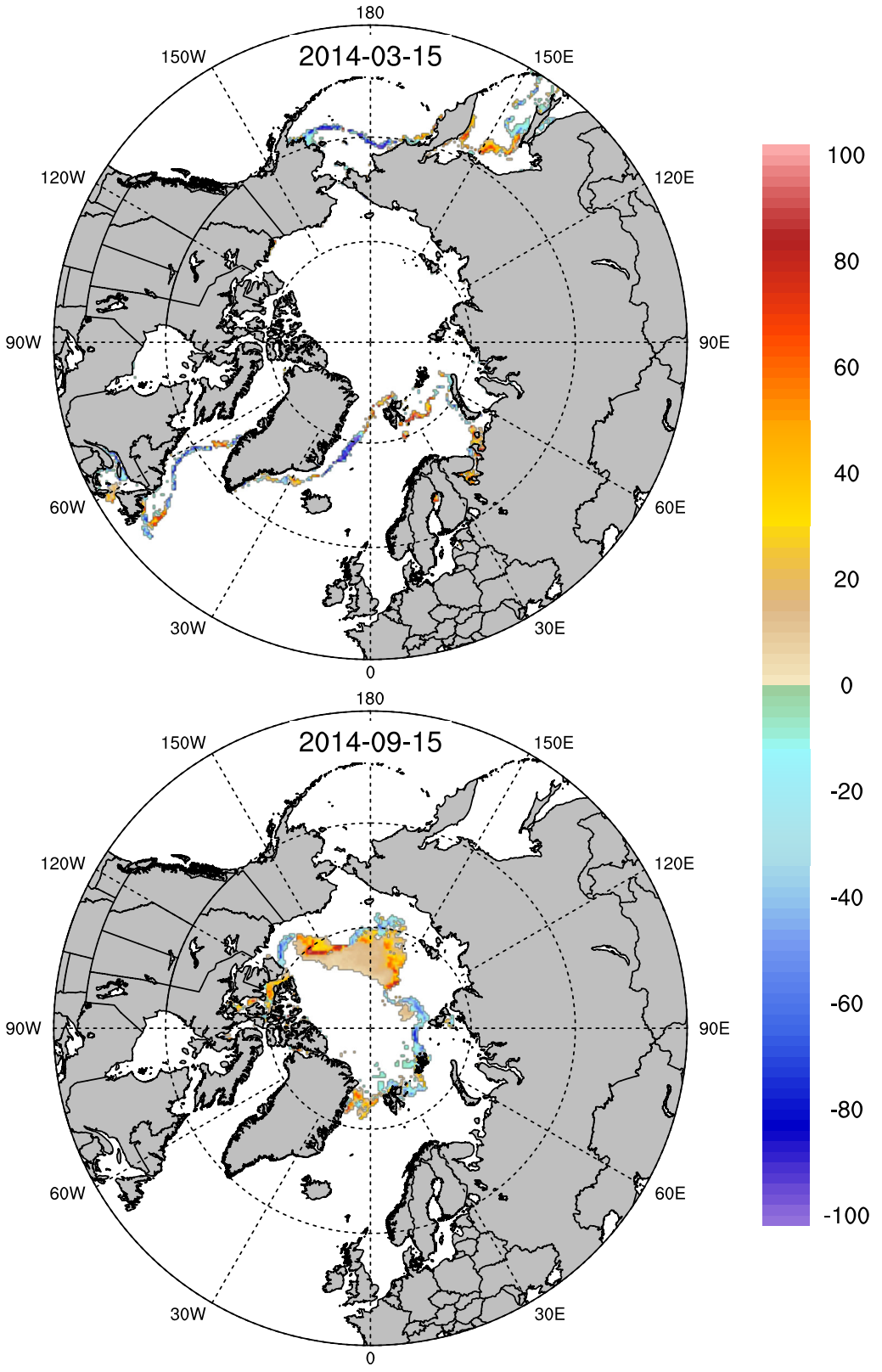

Figure 3. Areas where the assimilated ice concentration changes by more than ±5% for (top) 10–15 March 2014 and (bottom) 10–15 September 2014.

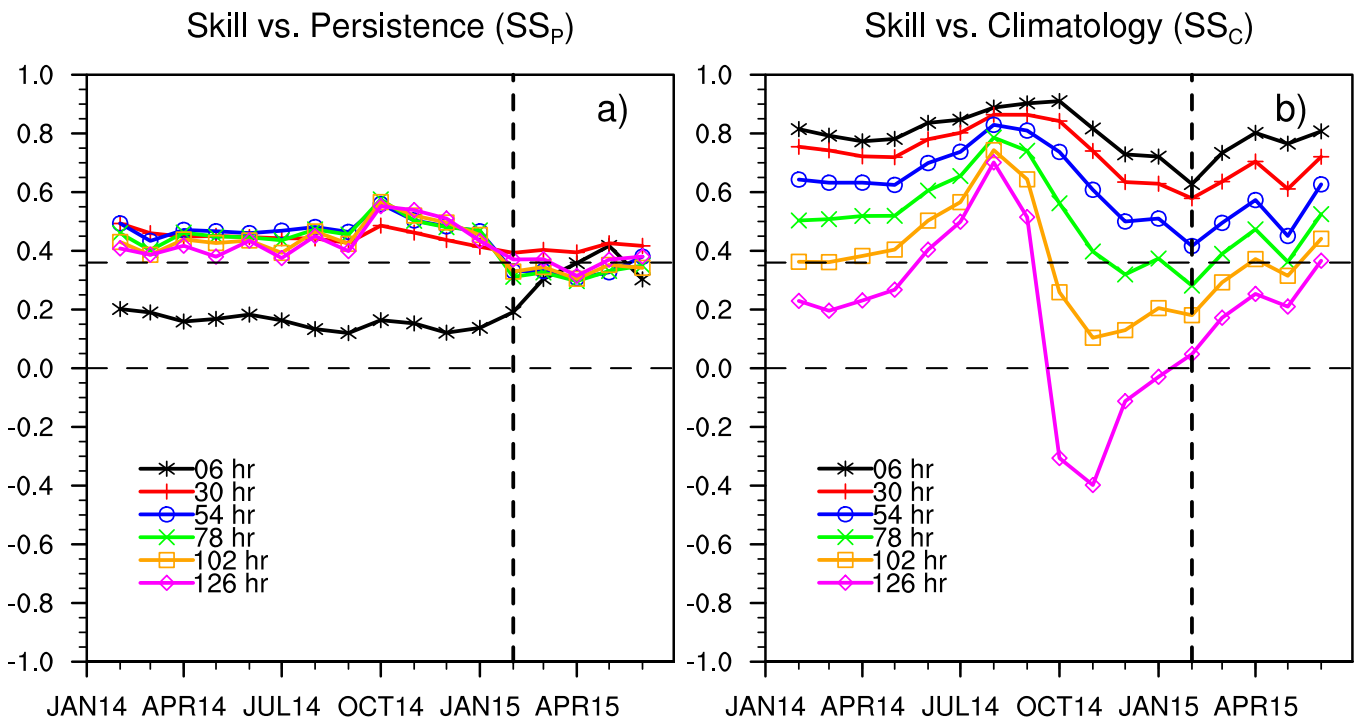

Figure 4. Skill scores relative to (a) persistence and (b) climatology. Scores above 0.0 show skill, scores above 0.36 are considered particularly **skilful**. The vertical dashed line is when ACNFS started assimilating ice concentration masked by IMS.

where the model ice concentration is less than 50%. Thus, in both plots of Figure 3, there are no locations of interest in the central ice pack since there was no assimilation of sea ice. In addition to limiting the number of points to those that change over the forecast, another advantage of this method is that the number of points used for each forecast on a particular day is the same (the number of points changes from day to day, however). Also, as noted in *Lemieux et al*. [2015], the CICE model is run at very high spatial resolution and produces linear kinematic features (LKFs) that are not seen in the lower resolution satellite observations. If the raw satellite data were to be used to locate points of interest, changes in the modeled LKFs would be missed. Thus, using the assimilated data to locate model points of change is more appropriate than the raw satellite observations. Since the points are based solely on the change in analysis field, without any consideration of the change in forecast field, points where the forecast changes by ±5% or more are not taken into account. As a result, our analysis does not take into account "false alarms" when the model forms ice where no ice forms in the analysis fields [*Van Woert et al*., 2004]. Daily skill scores were computed for the time period February 2014 to June 2015. The number of data points (not shown) varied from approximately 85,000 in the middle of September, during the minimum ice extent, to near 300,000 in May, when there is maximum ice area available to melt.

Figure 4 contains plots of the monthly mean SS_p and SS_c from the daily skill scores. In each plot there are two horizontal dashed lines at 0 and 0.36. Values above zero indicate model skill compared to the reference field, while values above 0.36 are considered to be particularly skilful [*Van Woert et al*., 2004]. The value 0.36 is chosen as corresponding to the selection of 0.6 correlation coefficient value as skilful in *Hollingsworth et al*. [1980]. In Figure 4a, SS_p is shown to always be above zero, indicating skill compared to assuming a persistent ice state. Also, all forecasts except the 6 h forecast are above 0.36, indicating good skill compared to persistence. The SS_p value below 0.36 for the 6 h forecast (prior to assimilation of AMSR2+IMS) is attributed to the relatively slow evolution of the ice concentration field, which typically does not change significantly in a 6 h period.

SS_c is also seen to be above zero in Figure 4b, with the exception of the 126 h forecast between September 2014 and January 2015. As one would expect, the longer the forecast the lower the skill score compared to climatology, as errors associated with the forecast increase. An interesting feature of this plot is that, based on this short 16 month analysis, SS_c tends to be cyclic, with higher scores in the summer months (July–September) up to the summer minimum ice extent and lower scores during the winter freeze up period of

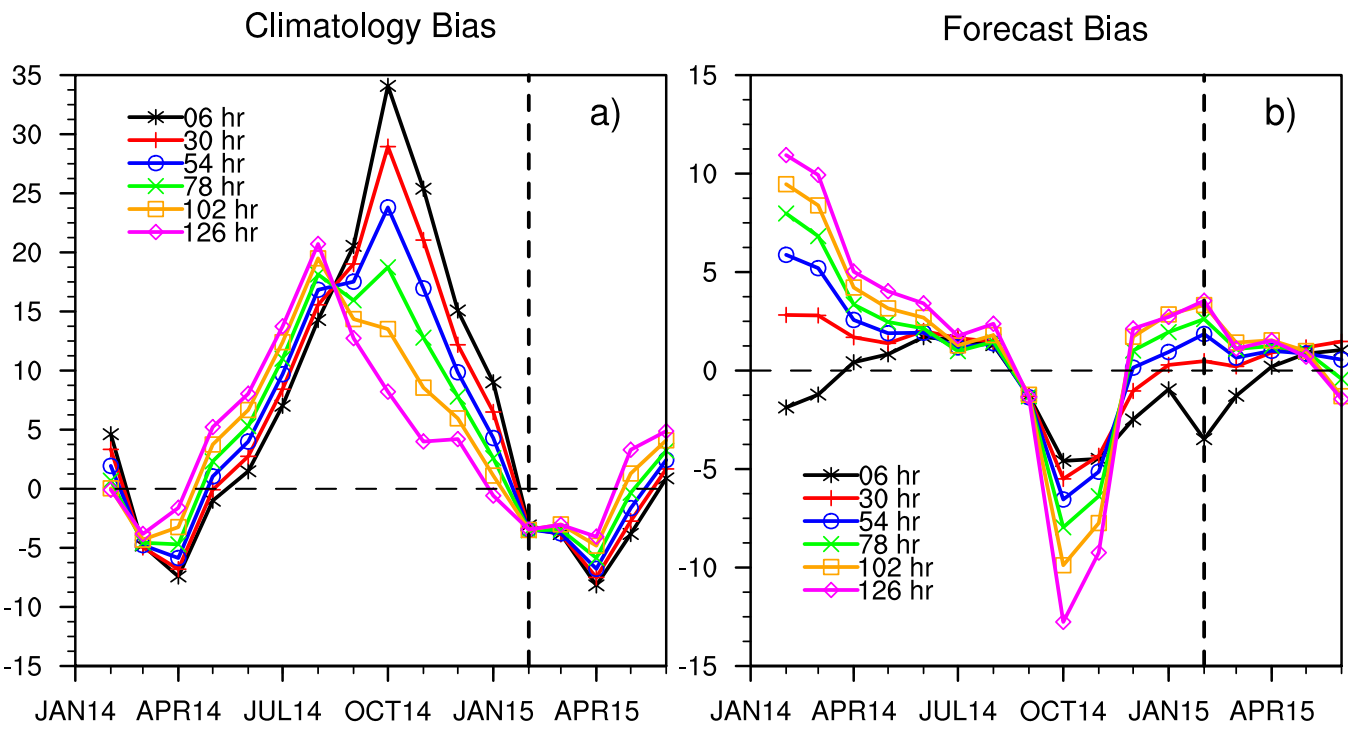

Figure 5. Monthly mean ice concentration (%) bias compared to the assimilated ice concentration for (a) climatology and (b) each forecast. The climatology bias is large in the winter months, indicating climatology has more ice than observations. The forecast bias is negative in the winter, indicating the model has less ice than observations. The vertical dashed line is when ACNFS first started to assimilate ice concentration masked with IMS.

October–January. The higher SS_c values in the summer suggest ACNFS does a good job at capturing ice melt, while degradation in SS_c during the freeze up period suggests that ACNFS may not form ice as fast as actually occurs in the Arctic.

In (5), the low SS_c in the winter can be attributed to either an increase in the forecast error or a decrease in the climatology error. Figure 5a depicts the bias between the climatological ice concentration and the assimilated value for that date, $(C_n - A_n)$, while Figure 5b is a plot of the bias between the model forecast and the assimilated value for that date, $(f_n - A_n)$. Here biases are examined instead of MSE to investigate the sign of the differences, since MSE in (3) is by definition a positive number. In Figure 5a, from May to January, the climatological bias is positive, indicating the climatology overestimates the ice concentration. This is in agreement with the observed decline in September sea ice minimum compared to climatology. It is interesting to note that in the melt period, May–September, the climatology bias increases with each forecast time. The increase in bias with forecast time occurs since, during the summer months, the ice is melting faster than seen in climatology. The converse is seen as the freeze season starts in October–January; the climatology bias decreases with forecast time as the ice grows and becomes closer to the climatology concentration. In contrast, the forecast bias (Figure 5b) during the winter freeze months of September–December is negative, indicating the model has less ice than the reference observation. The forecast bias becomes more negative with forecast time, indicating the model does not freeze ice as fast as observed. This, along with the reduction in climatology bias at each forecast time during the winter months, explains the degradation in SS_c during this time. Several possibilities exist to explain the large negative bias in forecast bias, ranging from perhaps too much incoming atmospheric radiation to warmer ocean temperatures to sea ice parameterizations. These will be the topic of a future study. We remind the reader that these biases are computed over the points where ice changes by $\pm 5\%$ over a 5 day period, and not the entire Arctic.

The assimilation of ice concentration with the blended AMSR2+IMS products was initiated in ACNFS on 2 February 2015. This date is marked as a vertical dashed line in Figures 4 and 5. The skill score versus persistence (SS_p) increased significantly for the 6 h forecasts, while SS_p remained virtually unchanged for the 30 h forecasts and dropped slightly for forecasts past 54 h. Since skill scores are a ratio of MSE's, the drop in the skill scores after 54 h forecast is caused here by a greater reduction in the persistence MSE compared to the

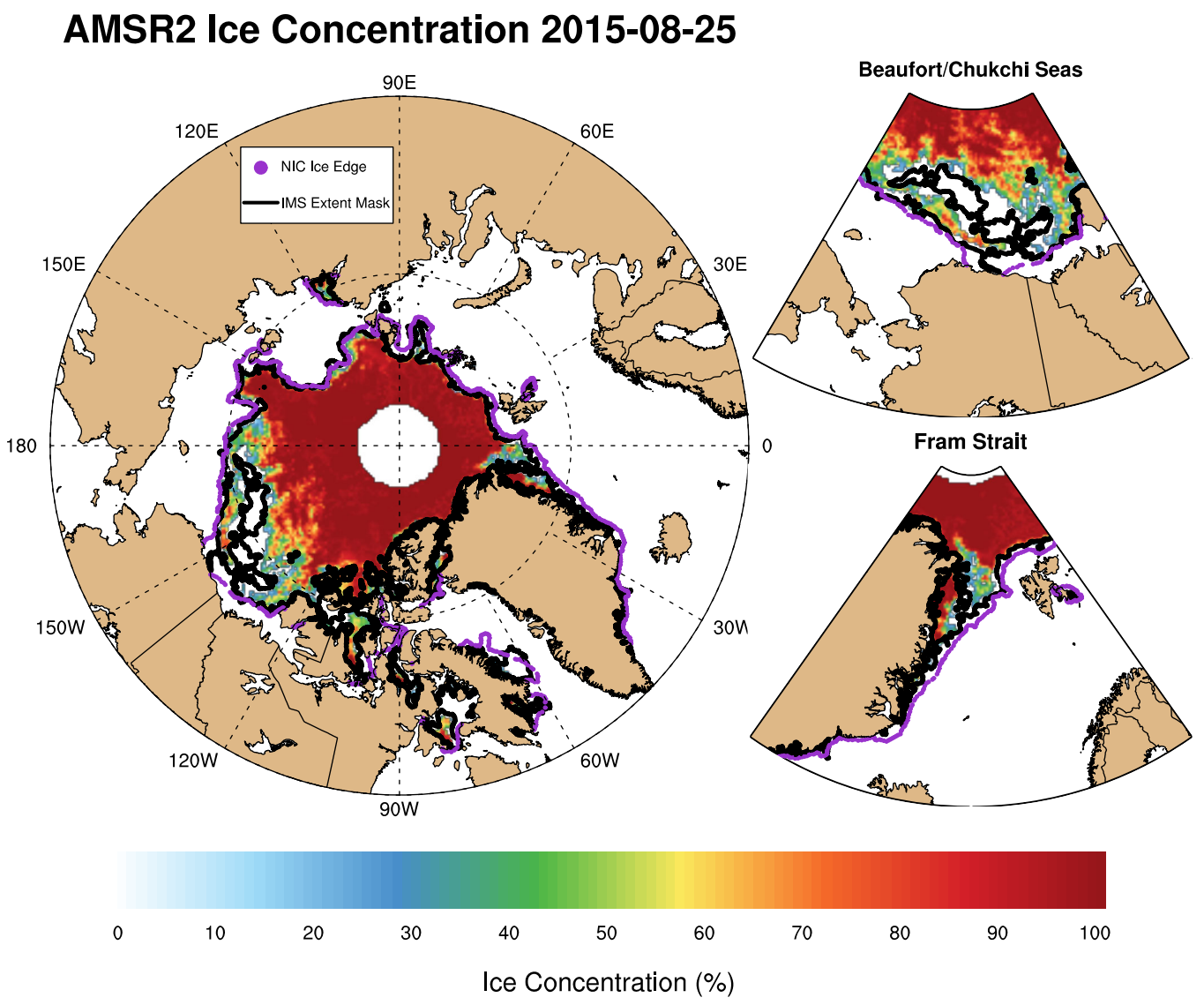

Figure 6. Difference between IMS and NIC Ice Edge Locations on 25 August 2015. The colored area is 10 km gridded ice concentration (%) from AMSR2. The black line is the IMS mask, and the purple dots are the NIC Ice Edge. The right plots contain the same data as the left, but are zoomed in to the Beaufort/Chuckchi Seas and the Fram Strait. The more conservative NIC Ice Edge location is almost always further south compared to IMS.

reduction in the forecast MSE (not shown). It is noted that the results with IMS are preliminary, as we have only been assimilating with the blended AMSR2+IMS for 4 months at the time of this writing. A longer-term study is needed to make more definitive conclusions regarding the impact of IMS assimilation.

3.2. Ice Edge Location

The NIC Ice Edge product is a product intended for navigational purposes to help vessels avoid nearly all ice hazards, and is created independently of the IMS product [*Helfrich et al.*, 2007; *Posey et al.*, 2015]. The NIC Ice Edge product is a series of latitude/longitude points defined where the ice concentration "varies between 0 and 1/10th" (S. Helfrich, NIC, personal communication 2014), and is a more conservative definition of ice edge compared to IMS ice extent The NIC Ice Edge product locations are determined by an analyst and typically utilizes different data sources, including satellite and *in-situ* observations, to determine the ice edge location compared to IMS. Figure 6 contains a representative plot of the difference between IMS and the NIC Ice Edge product. Here it is seen that the NIC Ice Edge product locations are almost always further south and contains more ice area than IMS. On this particular date shown in Figure 6, a polynya is seen in the Beaufort/Chukchi seas and is identified by IMS, whereas the NIC Ice Edge product encompasses the entire polynya region. Since the NIC Ice Edge product locations are not assimilated into ACNFS, we compare

the distance between the NIC Ice Edge product locations and the ice edge location derived from ACNFS. (See *Posey et al*. [2015] for a more detailed discussion of the differences between the NIC Ice Edge product and IMS ice extent.)

In this study the ACNFS ice edge is defined as those points that exceed a specified threshold value for ice concentration that also have a neighboring point that falls below this threshold value. The midpoint of the NIC Ice Edge product ice concentration definition, 5%, is used as the ACNFS ice concentration threshold. Thus, any model grid cell with ice concentration greater than 5% that also has an adjacent cell with ice concentration less than 5% is identified as the model ice edge. After determining the ACNFS ice edge, the next step is to identify the ACNFS model grid point that contains the NIC Ice Edge product location. The closest ACNFS ice edge point to the NIC Ice Edge product location is found, and the distance between the two points is then computed using via the Haversine formula [*Gade*, 2010, equation (19)]

$$D_e = 2r \arcsin\left(\sqrt{\sin^2\left(\frac{\Phi_1-\Phi_0}{2}\right)+\cos(\Phi_0)\cos(\Phi_1)\sin^2\left(\frac{\Theta_1-\Theta_0}{2}\right)}\right) \tag{7}$$

Here r is the radius of curvature of the Earth, Φ and Θ are latitude and longitude (respectively) in radians, and the subscripts 0, 1 indicate either ACNFS ice edge or NIC Ice Edge, respectively. Assuming the Earth to be an ellipsoid, the radius of curvature is dependent on latitude and computed as in *Snyder* [1987, equations (4)–(18)]:

$$r = \frac{a(1-e^2)}{1-e^2\ \sin^2(\Phi)} \tag{8}$$

where a=6378137.0 m is the semi-major axis length of the Earth, e=8.181919 $\times$ 10^{-2} is the Earth's eccentricity obtained from WGS84 standard [*NIMA*, 2000], and Φ is the average latitude between the two ice edge points. The value of D_e in (7) is an absolute value of the distance between NIC Ice Edge product location and ACNFS ice edge is used for analysis. Thus, there is no signed value to indicate if the ACNFS ice edge extent is more or less than the NIC Ice Edge product location. Since there may be a spatial dependence on the ice edge difference, daily mean ice edge distances for seven regional seas are computed: Central Arctic, Greenland-Iceland-Norwegian (GIN) Seas, Barents Sea, Laptev Sea, Sea of Okhotsk, Chukchi Sea, and the Canadian Archipelago (Figure 7a).

The ice edge error results for the entire time of this study, February 2014 to June 2015, are shown in Figure 7b. The forecast ice edge distance error is shown in solid lines, while the ice edge distance error from persistence is shown in the dashed lines. Here it is seen that persistence has similar or lower ice edge errors compared to the forecasts. The lower error by assuming persistence indicates the modeled ice edge in ACNFS evolves more rapidly than in the Arctic, and the modeled error is greater than assuming a persistent ice state (this changes with the assimilation of IMS, discussed below). Overall, the ice edge errors range from near 30 km at 6 h forecast to over 80 km for 126 h forecast. As expected, the ice edge error distance increases as forecast time increases. Depending on the region, the forecast edge error increases by 10 km (Barents Sea) to 20 km (Canadian Archipelago) over the forecast period. The Canadian Archipelago, with the presence of many small straits and landmasses, is the most challenging of regions to model, and thus it is expected this region will have the highest ice edge error.

To look at the effect of assimilating the blended AMSR2+IMS on the ice edge error, Figure 7c is a plot of ice edge error for the months February–June 2014, before ACNFS started to assimilate the blended product, while Figure 7d is a plot of ice edge error for the same months when ACNFS assimilated the blended AMSR2+IMS product, February–June 2015, for comparison. In Figure 7d, the influence of assimilating the blended AMSR2+IMS can be seen, the forecast ice edge is closer to the NIC Ice Edge and errors using AMSR2+IMS are lower than persistence for all regions except the Canadian Archipelago 102 h and 126 h forecasts. It is interesting that in Figure 7d, the forecast ice edge error (solid lines) decreases through the first 54 h. This decrease can be explained by noting that the months of the study with AMSR2+IMS (February–June), the ice is retreating. Since the IMS is not as conservative in identifying the ice edge as the NIC Ice Edge (Figure 6), the ACNFS initial extent using AMSR2+IMS is less than the NIC Ice Edge. As time evolves, the daily NIC Ice Edge location would be retreating faster than the model, causing the ice edge comparison to improve with time. Although this pattern is encouraging, it is also noted that in some regions the initial magnitude of the error increased by 5–10 km compared to not assimilating AMSR2+IMS, including the GIN

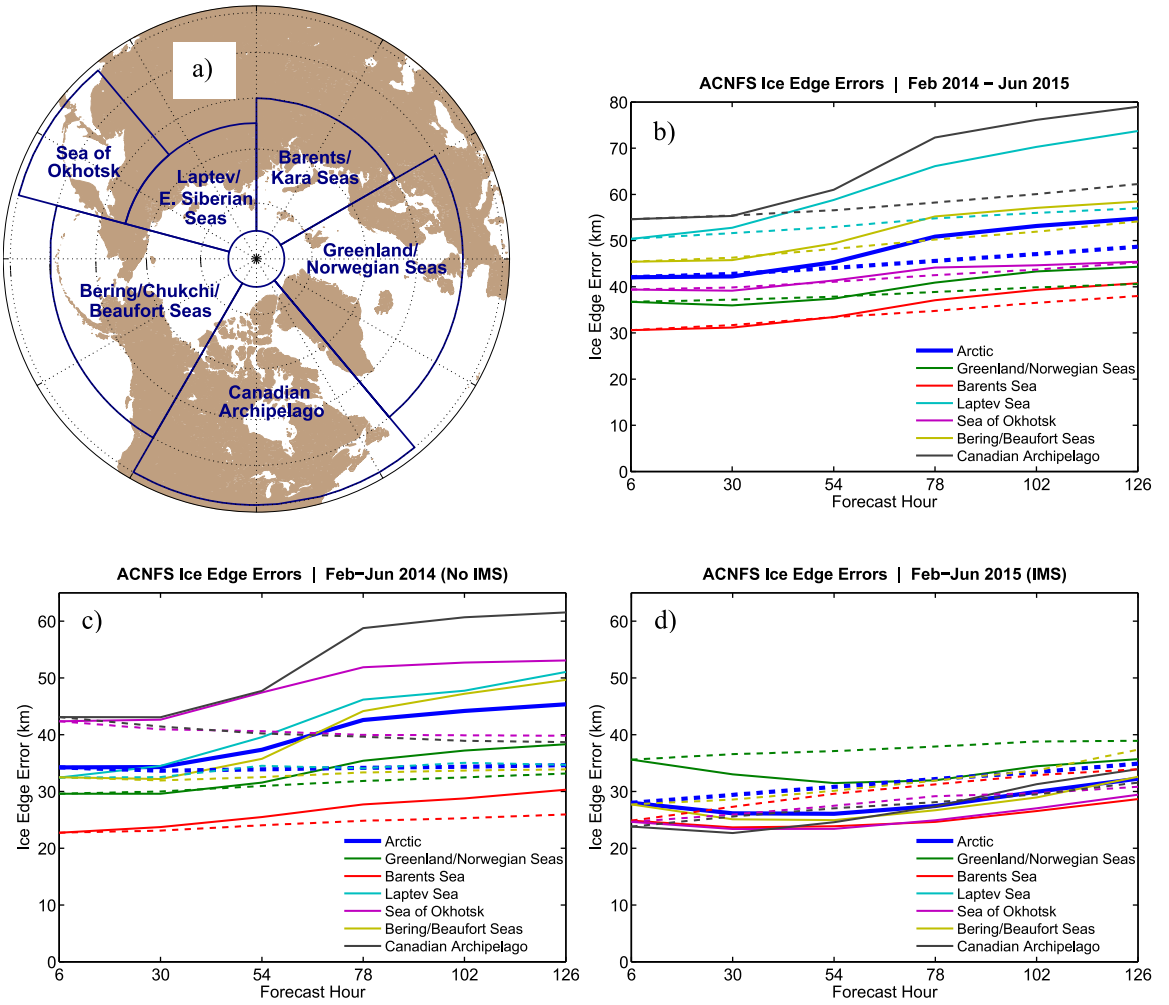

Figure 7. (a) Regions defined for the ice edge analysis. (b) Average ice edge forecast error (km) compared to the NIC ice edge for each region. (c) Same as Figure 7b but from February to June 2014 (without IMS). (d) Same as Figure 7c but from February to June 2015 (with IMS). Solid lines represent forecast error, dashed lines represent persistence error. Note the change in vertical axis from Figure 7b to Figures 7c and 7d.

Seas and Barents Sea (although the initial error value increased, the actual change in error over the 126 h forecast was roughly the same for each region). This increase in ice edge error is on the order of 2–5 ACNFS grid points and could be a result of inter-year model variability or NIC Ice Edge location variability (recall the NIC Ice Edge is generated via human analyst, and analysis by person can vary) [*Posey et al.*, 2015].

3.3. Ice Drift

In addition to forecasting the ice edge location, it is of interest to forecast ice motion. This is important for predicting where the ice is heading, and is particularly useful for navigation planning purposes. Here we compare the ACNFS ice velocity and separation distance to data obtained from the International Arctic Buoy Programme (IABP). IABP is a network of drifting buoys in the Arctic Ocean to provide meteorological and oceanographic data for real-time operational requirements and research purposes; data are made available to the public at http://iabp.apl.washington.edu. For the time period of this study, 377 buoys were used. Two quantities are investigated: (1) ice drift speed and (2) separation distance error. For each quantity the forecast differences are compared to values obtained if persistence was assumed. Each is described further below.

3.3.1. Drift speed

The IABP speed is determined by the distance the buoy traveled over 24 h. The distance the buoy traveled, D_b, is obtained via the Haversine formula defined in (7), but with a slight modification of the latitude and longitude subscripts:

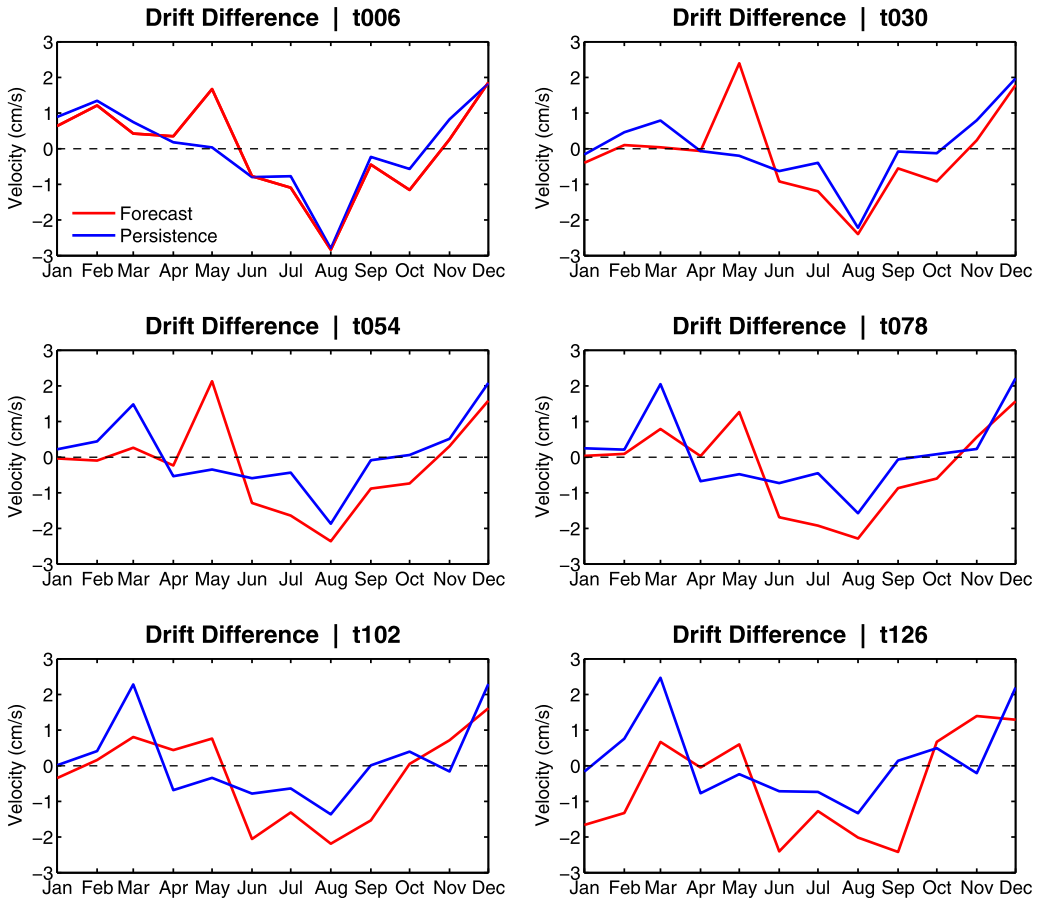

Figure 8. Monthly mean ice drift speed difference (cm/s) between IABP and ACNFS. Blue line is persistence difference, red line is forecast difference. The monthly means were computed from all available IABP drifters in that month. The model restart ice velocity is used as the reference state for persistence. The forecast time (tau) is noted in the title of each plot. The location of the IABP was linearly interpolated to the ACNFS grid to obtain the ACNFS ice drift speed.

$$D_b = 2r \arcsin\left(\sqrt{\sin^2\left(\frac{\Phi_{24}-\Phi_0}{2}\right)+\cos(\Phi_0)\cos(\Phi_{24})\sin^2\left(\frac{\Theta_{24}-\Theta_0}{2}\right)}\right) \tag{9}$$

Here the subscripts 0, 24 indicate the buoy starting position time and position time 24 h later, respectively, and all other terms are defined as in (7) and (8). The speed of the buoy in meters/second is then D_b divided by 86,400 seconds per day:

$$S_b = \frac{D_b}{86400} \tag{10}$$

Here we note that S_b is a mean speed over 24 h. In contrast, the velocity fields written by ACNFS are instantaneous, and not a daily average. In order to define a modeled speed that is similar to a daily mean, an average of the modeled output velocity fields, u and v, at the start of the analysis time and that 24 h later was computed:

$$S_m = \sqrt{\bar{u}^2+\bar{v}^2} \tag{11}$$

Here the overbar represents the average of the current velocity and the velocity 24 h later. It is important to note that, due to the fact that ice velocity is highly dependent on the atmospheric stress applied, and that stress is provide from NAVGEM every 3 h, there is an error associated with computing the average only from instantaneous outputs 24 h apart.

In order to compare the modeled and IABP speeds, the first step is to obtain the model grid cell containing the buoy location at the particular model output date. The difference between the model forecast ice speed

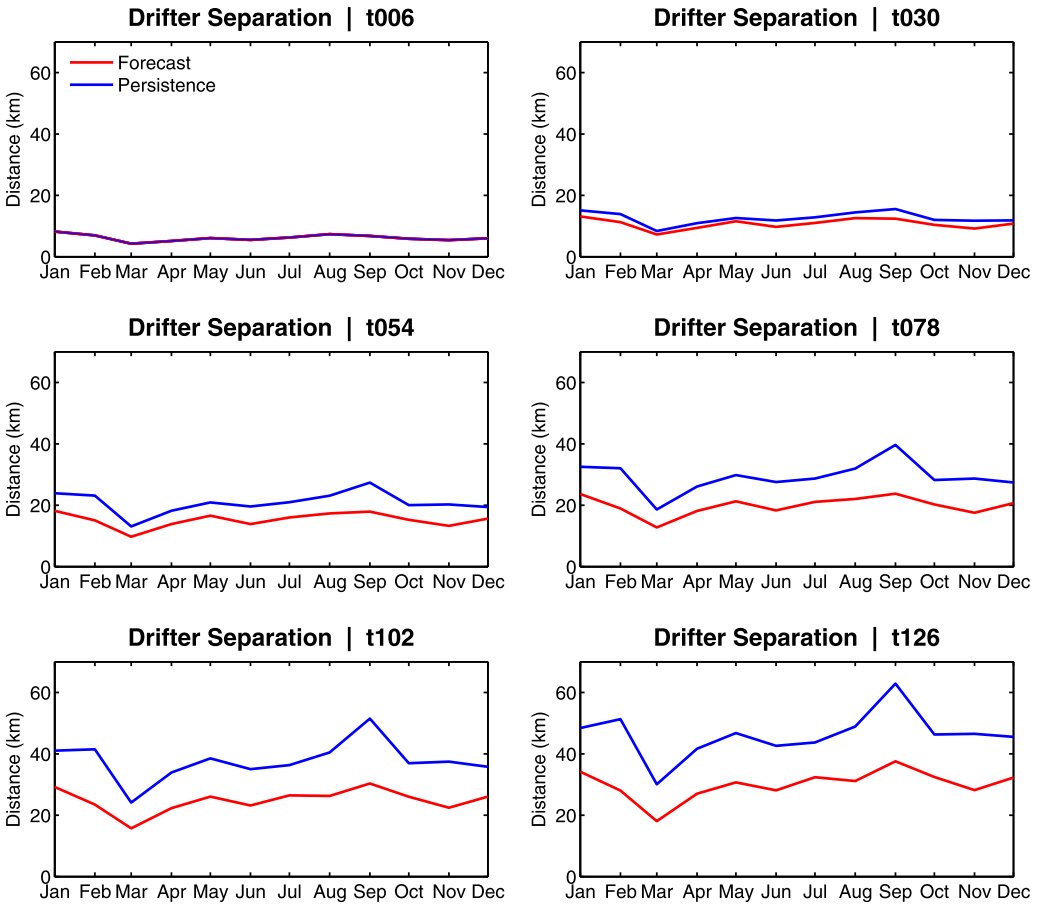

Figure 9. Monthly mean 24 h drifter separation distance (km) between forecast (red) and persistence (blue) buoy positions starting at each forecast tau. The forecast separation analysis starts with the 6 h forecast time since IABP data are available at 00Z. As a result, the 6 h forecast velocity is used for persistence. Starting with 6 h forecast, the location of the IABP buoy is found in ACNFS, then the ACNFS velocity (forecast or persistence) is applied for 24 h. The difference between the modeled position and actual IABP position 24 h later is then computed. Then at the 30 h forecast, the modeled ice drift is applied for 24 h to the resulting position from the 6 h forecast. The new result is compared to the IABP position 24 h later. The process is continued for all forecast times.

and buoy ice speed, $\Delta_f = S_m^f - S_b^f$, is then computed for each forecast time (here f is the forecast hour). In addition, the speed difference is computed by assuming a persistent ice state from the forecast initialization, $\Delta_p = S_m^0 - S_b^f$, where the superscript "0" indicates the forecast initialization. Figure 8 contains the monthly mean Δ_f (red line) and Δ_p (blue line) for each forecast time. For all the forecast times the model is slower than the buoy speed in the summer and autumn months (June–October), with a max velocity difference around -2 cm/s in August. In contrast, the winter and spring months (November–May) the model is faster than the buoys, except for April past 54 h. It is also interesting to note that during summer and autumn, persistence performs better than the forecast for forecast times at and beyond 54 h, while for the winter and spring months the opposite is generally the case. Since ice drift is largely driven by wind and ocean stresses, these results suggest that there may be seasonality biases in the wind forcing or air-ice/ocean-ice drag coefficients. This will be the topic of a future study.

3.3.2. Drifter separation

The drifter separation difference is the distance between the actual drifter position and the projected position using the ACNFS velocity field for each forecast period. Since the distance traveled is dependent on the length of forecast time, a comparison with equal spaced times is desired. Also, since the IABP buoy locations are reported twice per day at 00Z and 12Z, it is convenient to start the analysis with the 6 h forecast instead of the initial velocity field. This avoids the need to interpolate the IABP position to the model restart time (18Z). Therefore, the drifter location comparisons were started with the 6 h forecast and made with every subsequent 24 h forecast. This was accomplished by first identifying the location of the buoy at the 6 h forecast time. The ACNFS forecast velocity at this location was obtained by making a triangular interpolant of

the ACNFS grid, then applying a "natural neighbor" interpolation scheme [*Ledoux and Gold*, 2005]. The projected position of the virtual buoy is then "forecast" using the ACNFS velocity at this time for the next 24 h, and the distance between this forecast location and the actual buoy location is computed. The process is repeated for the next 24 h period, using the velocity from the forecast position (i.e., not the actual buoy location) to update the forecast buoy position. Note that as defined in (11), the forecast velocity applied at each period is an average of the current velocity and the velocity 24 h later, not the instantaneous velocity field. In addition to the forecast distance, the position difference was computed by assuming a persistent velocity using the 6 h forecast field for the entire 126 h forecast period.

Figure 9 contains the monthly averaged distances between observed and forecast buoy location. For the 6 h forecast, the buoy distance is about 6 km for both persistence and forecast velocities (recall that the 6 h forecast is the reference time, thus the results are the same for both forecast and persistence). As forecast time increases, the distance between modeled and actual buoy location increases. The forecast error is lower than when assuming persistence, reaching an average of 30 km by the 126 h forecast compared to an average distance error of 45 km by assuming persistence. This is in contrast to the ice velocity differences shown in Figure 8, where persistence out-performed forecast velocity, especially in the summer months. Even though the model was slower than persistence, the better performance by the forecast in the drifter distance analysis is due to the inclusion of the direction of the ice drift in each forecast. Since the forecast drift adapts with time compared to persistence, the modeled forecast location is closer to the actual buoy location than assuming a persistent ice state. Similar to the speed difference above, the largest distance error seems to be in the summer and autumn months. Factors that influence the forecast separation are the atmospheric forcing and drag coefficients, as well as potential biases in ice seasonal ice thickness and ice strength that could lead to bias in drift speed [*Zhang et al.*, 2012], and will be examined with a longer-term study.

4. Summary

Forecast skill can broadly be thought of as any improvement the model provides relative to assuming some baseline condition. Two baseline conditions are considered in this study: persistence (assuming conditions do not change over the forecast time), and climatology (historical averages). In determining ACNFS forecast skill, we are interested mainly in the marginal ice zone where the ice concentration changes the fastest with time. Therefore, forecast skill was computed only where the assimilated ice concentration changed by more than $\pm 5\%$ over a 5 day period. This captures areas of ice growth and melt, and is limited mostly to the marginal ice zone (Figure 3). Starting in February 2015, ACNFS began to assimilate a blended AMSR2+IMS product. The effect on skill scores with this new data set is also examined.

Overall, ACNFS demonstrates a high level of skill compared to persistence, with SS_p values above zero for the entire time of this study (Figure 4a). Only the 6 h SS_p is below 0.36. Over a 6 h period the ice conditions are not expected to change much, thus the skill at 6 h compared to persistence is expected to be lower. One would expect SS_p to increase as the forecast time increases, but that is not the case here; at the 30 h forecast point and beyond SS_p hovers around $0.4 - 0.5$. While this still indicates the forecasts are better than assuming a persistent ice state, further investigation as to why the SS_p does not increase past 30 h is needed. The inclusion of IMS to the assimilated NCODA ice concentration improved the 6 h SS_p to about 0.4, making it "particularly skilful." Unfortunately, the inclusion of IMS seemed to have little effect on the other forecast times. Since this was only performed for a 4 month period, a longer study is needed to evaluate any potential biases throughout the year.

The skill score compared to climatology, SS_c, behaves as one would expect, with SS_c the highest for the 6 h forecast and decreases with forecast time (Figure 4b). SS_c is positive for all forecast times except for the winter months of the 126 h forecast, and thus performs better than assuming a climatological ice concentration. SS_c can be affected by inter-annual variation in sea ice cover. If the sea ice concentration of a particular year happens to be close to climatology, then SS_c will be lower, since $MSE(C_n, A_n)$ in (5) will decrease. Conversely, SS_c will increase if the ice concentration departs greatly from climatology. In order to examine the dip in SS_c from October to January, the climatology and forecast biases are examined (Figure 5). In Figure 5a, the climatology is shown to be biased higher than the assimilated ice concentration during May–January, as one would expect given the increased rate of summer sea ice extent decline. The climatology bias decreases with forecast time from October to January (Figure 5a), as the model starts to form more ice

and become close to the climatology value. The bias in forecast ice concentration increases with forecast time (Figure 5b) during the same time, indicating that model does not form ice as quickly as observed. Several possibilities exist to explain the large negative bias in forecast bias, ranging from perhaps too much incoming atmospheric radiation to warmer ocean temperatures to sea ice parameterizations. Since the skill score is the ratio of the MSE of these terms, the combination of these facts is causing the skill score to degrade during this time for the longer forecasts. Also, by defining the points of interest to be where the assimilated ice concentration differs by greater than $\pm 5\%$ over a 5 day period, the comparison is limited to near the ice edge and does not indicate model skill compared to climatology for the full Arctic.

Regarding SS_c, the sea ice climatology used in this analysis was created from ECMWF data for the years 1979–1996. As noted in the introduction, the past few decades have seen a greater reduction in September mean ice extent compared to earlier decades. While the use of this climatology was consistently used to quality control the ice observations, it is possible that using a more recent climatology from either ECMWF or the National Centers for Environmental Prediction (NCEP) could have an impact on SS_c.

The location of the sea ice edge is important for operational planning of science and maritime activity. In this study the forecast ACNFS ice edge (defined as 5% ice concentration) is compared to the independently obtained NIC Ice Edge product locations. The analysis was divided into 7 regions (Figure 7a). ACNFS performed best in the Barents Sea region, with ice edge error ranging from 30 km at 6 h forecast to 40 km at 126 h forecast, and worst in the Canadian Archipelago, with ice edge errors ranging from 60 km at 6 h forecast to 80 km at 126 h forecast. With many small openings and landmasses in the Canadian Archipelago, this region is perhaps the most difficult to model. In order to examine the effect of assimilating IMS, Figures 7c and 7d contain plots of the ice edge error for the same length of time (February–June) before and after assimilating AMSR2+IMS. Here it is seen that the inclusion of AMSR2+IMS reduced the ice edge error compared to the non-IMS period. In Figure 7d the error is also seen to decrease with time up to the 54 h forecast. This is a consequence of the IMS field not defined as conservative as the NIC Ice Edge locations (Figure 6). During this spring ice retreat, as forecast time lengthens the NIC Ice Edge locations will move closer to the IMS location, causing the ice edge error stats to improve.

In addition to ice concentration, ice speed and buoy separation distance were compared to data reported from IABP buoys. Overall, the ice velocity in ACNFS was slower than IABP buoys in the summer months of June–October (Figure 8). During this time, assuming a persistent ice speed performed better by as much as 1.5 cm/s for the September 126 h forecast. In contrast, the modeled velocity was greater than observed for the March–May time frame. This suggests a seasonal bias to either the wind or drag coefficients. This could occur as a result of the change in surface conditions. For instance, in the summer months most of the snow has melted and could result in a rougher surface than when snow exists and fills surface ridges and cracks. This change would not be taken into account in ACNFS, and the wind stress could be underestimated.

In addition to ice velocity, a virtual IABP buoy was modeled by starting at the same position as the real IABP buoy, but advected using the ACNFS forecast ice drift velocities. In contrast to the velocity difference, the modeled drifter separation distance was smaller for each forecast compared to persistence. This implies that while the ACNFS ice speed may be slower or faster during a particular time, the forecast ice direction is closer to reality than if a persistent ice speed and direction are assumed.

Acknowledgments

IABP data are made available to the public at http://iabp.apl.washington.edu. AMSR2 data are available after registration at GCOM-W1 data server site https://gcom-w1.jaxa.jp. IMS and NIC ice edge products are available from the NIC web site http://www.natice.noaa.gov/Main_Products.htm. ECMWF sea ice concentration data are available via http://www.ecmwf.int/en/research. This work was funded as part of the Naval Research Laboratory's 6.1 Research Option "Determining the Impact of Sea ice Thickness on the Arctic's Naturally Changing Environment" (DISTANCE). Numerical simulations were performed at the Navy Department of Defense Supercomputing Resource Center (DSRC) using grants from the Department of Defense High Performance Computing Modernization Program. All model data are securely stored at the Navy DSRC archive server. The files stored there can be accessed after obtaining an account at the facility. The corresponding author can be contacted for information to access the archived data once an account has been established. The authors thank Axel Schweiger and Jean-François Lemieux for their comments leading to several improvements in this paper.

References

Arrigo, K., G. van Dijken, and S. Pabi (2008), Impact of a shrinking Arctic ice cover on marine primary production, *Geophys. Res. Lett.*, *35*, L19603, doi:10.1029/2008GL035028.

Aschan, M., and R. Ingvaldsen (2009), Recruitment of shrimp (Pandalus borealis) in the Barents Sea related to spawning stock and environment, *Deep Sea Res., Part II*, *56*(21-22), 2012–2022, doi:10.1016/j.dsr2.2008.11.012.

Bertino, L., and K. A. Lisæter (2008), The TOPAZ monitoring and prediction system for the Atlantic and Arctic Oceans, *J. Oper. Oceanogr.*, *11*(2), 15–18.

Bitz, C. M., and W. H. Lipscomb (1999), An energy-conserving thermodynamic model of sea ice, *J. Geophys. Res.*, *104*(C7), 15,669-15,677, doi:10.1029/1999JC900100.

Bleck, R. (2002), An oceanic general circulation model framed in hybrid isopycnic-Cartesian coordinates, *Ocean Modell.*, *4*(2), 219–219, doi:10.1016/S1463-5003(01)00017-8.

Buehner, M., A. Caya, L. Pogson, T. Carrieres, and P. Pestieau (2013), A new environment Canada regional ice analysis system, *Atmos. Ocean*, *51*(1), 18–34, doi:10.1080/07055900.2012.747171.

Campbell, T., et al. (2010), Integrated modeling of the battlespace environment, *IEEE Comput. Sci. Eng.*, *12*(5), 36–45, doi:10.1109/MCSE.2010.78.

Carnes, M., R. W. Helber, C. N. Barron, and J. M. Dastague (2010), Validation test report for GDEM4. *Tech. Rep. NRL/MR/7330–10-9271*, Naval Res. Lab., Stennis Space Center, Hancock, Miss.

Cayula, J-F. P., D. A. May, B. D. McKenzie, K. D. Willis (2013), VIIRS-derived SST at the Naval Oceanographic Office: From evaluation to operation, in W. W. Hou and R. A. Arnone, *Proceedings of SPIE 8724 on Ocean Sensing and Monitoring V*, vol. 8724, 87240S–87240S-8, SPIE, Baltimore, Md., doi:10.1117/12.2017965.

Chassignet, E., L. Smith, G. Halliwell, and R. Bleck (2003), North Atlantic Simulations with the Hybrid Coordinate Ocean Model (HYCOM): Impact of the vertical coordinate choice, reference pressure, and thermobaricity, *J. Phys. Oceanogr.*, *33*(12), 2504–2526, doi:10.1175/1520-0485(2003)033 < 2504:NASWTH>2.0.CO;2.

Comiso, J. C. (1986), Characteristics of winter sea ice from satellite multispectral microwave observations, *J. Geophys. Res.*, *91*(C1), 975–994.

Comiso, J. C. and F. Nishio (2008), Trends in sea ice cover using enhanced and compatible AMSR-E, SSM/I, and SSMR data. *J. Geophys. Res.*, *113*, C02S07, doi:10.1029/2007JC004257.

Cox, M. (1984), A primitive equation, 3-dimensional model of the ocean, GFDL Ocean Group technical report 1, Geophys. Fluid Dyn. Lab., Princeton, N. J.

Cummings, J. (2011), Ocean data quality control, in *Operational oceanography in the 21st Century*., edited by A. Shiller and G. Brassington, pp. 91–122, Springer, Dordrecht, Netherlands.

Cummings, J. A. (2005), Operational multivariate ocean data assimilation, *Q. J. R. Meteorol. Soc.*, *131*(613), 3583–3604, doi:10.1256/qj.05.105.

Cummings, J. A., and O. M. Smedstad (2013), Variational data assimilation for the global ocean, in *Data Assimilation for Atmospheric, Oceanic and Hydrologic Applications*, vol. II, edited by S. K. Park and L. Xu, pp. 303–343, Springer, Berlin, doi:10.1007/978-3-642-35088-7_13.

Durner, G., J. Whiteman, H. Harlow, S. Amstrup, E. Regehr, and M. Ben-David (2011), Consequences of long-distance swimming and travel over deep-water pack ice for a female polar bear during a year of extreme sea ice retreat, *Polar Biol.*, *34*(7), 975–984, doi:10.1007/s00300-010-0953-2.

Fenty, I., and P. Heimbach (2013), Coupled sea ice-ocean-state estimation in the Labrador Sea and Baffin Bay, *J. Phys. Oceanogr.*, *43*(5), 884–904, doi:10.1175/JPO-D-12-065.1.

Fernandez, P., G. Kelly, and R. Saunders (1998), Use of SSM/I ice concentration data in the ECMWF SST analysis, *Meteorol. Appl. 5*(4), 287–296, doi:10.1017/S1350482798000942.

Fetterer, F., M. Savoie, S. Helfrich, and P. Clemente-Colón (2010), *Multisensor Analyzed Sea Ice Extent-Northern Hemisphere (MAISE-NH)*, National Snow and Ice data Center, Boulder, Colo., doi:10.7265/N5GT5K3K.

Fetterer, F., J. S. Stewart, and W. N. Meier (2015), *MASAM2: Daily 4-km Arctic Sea Ice Concentration, 2012-2014*, Natl. Snow and Ice Data Cent., Boulder, Colo., doi:10.7265/N5ZS2TFT.

Fox, D. N., W. J. Teague, C. N. Barron, M. R. Carnes, and C. M. Lee. The Modular Ocean Data Assimilation System (MODAS) (2002), *J. Atmos. Oceanic Technol.*, *19*(2) 240–252, doi:10.1175/1520-0426(2002)019 < 0240:TMODAS>2.0.CO;2.

Gade, K. A (2010), Non-singular horizonal position representation. *J. Navig.*, *63*, 395–417, doi:10.1017/S0373463309990415.

Gao, G., C. Chen, J. Qi, and R. Beardsley (2011), An unstructured-grid, finite-volume sea ice model: Development, validation, and application, *J. Geophys. Res.*, *116*, C00D04, doi:10.1029/2010JC006688.

Helfrich, S. R., D. McNamara, B. H. Ramsay, T. Baldwin, and T. Kasheta (2007), Enhancements to, and forthcoming developments in the Interactive Multisensor Snow and Ice Mapping System (IMS), *Hydrol. Processes*, *21*(12), 1576–1586, doi:10.1002/hyp.6720.

Hibler, W. D. (1979), Dynamic thermodynamic sea ice model, *J. Phys. Oceanogr.*, *9*(4), 815–846, doi:10.1175/1520-0485(1979)009 < 0815:ADTSIM>2.0.CO;2.

Hibler, W. D. (1980), Modeling a variable thickness sea ice cover, *Mon. Weather Rev.*, *108*(12), 1943–1973, doi:10.1175/1520-0493(1980)108 < 1943:MAVTSI>2.0.CO;2.

Hill, C., C. DeLuca, Balaji, M. Suarez, and A. da Silva (2004), The architecture of the earth system modeling framework, *Comput. Sci. Eng.*, *6*(1), 18–28, doi:10.1109/MCISE.2004.1255817.

Hogan, T. F., T. E. Rosmond, and R. Gelaro (1991), The description of the navy operational global atmospheric prediction system, *NOARL Rep. 13*, Naval Res. Lab., Stennis Space Cent., Hancock, Miss.

Hogan, T. F., et al. (2014), The Navy Global Environmental Model, *Oceanography*, *27*(3), 116–125.

Hollinger, J. P. (1991), *DMSP Special Sensor Microwave Imager Calibration/Validation—Final Report Volume II*, Naval Res. Lab., Washington, D. C.

Hollingsworth, A., K. Arpe, M. Tiedtke, M. Capaldo, and H. Savijarvi (1980), The performance of a medium-range forecast model in winter-impact of physical parameterizations, *Mon. Weather Rev.*, *108*(11), 1736–1773, doi:10.1175/1520-0493(1980)108 < 1736:TPOAMR>2.0.CO;2.

Hunke, E., and W. Lipscomb (2008), CICE: The Los Alamos Sea Ice Model documentation and software user's manual version 4.0, *Tech. Rep. LA-CC-06-012*, Los Alamos Natl. Lab., Los Alamos, N. M.

Hunke, E. C., and J. K. Dukowicz (1997), An elastic-viscous-plastic model for sea ice dynamics, *J. Phys. Oceanogr.*, *27*(9), 1849–1867, doi:10.1175/1520-0485(1997)027 < 1849:aevpmf>2.0.co;2.

Hunke, E. C., and J. K. Dukowicz (2002), The elastic-viscous-plastic sea ice dynamics model in general orthogonal curvilinear coordinates on a sphere-incorporation of metric terms, *Mon. Weather Rev.*, *130*(7), 1848–1865, doi:10.1175/1520-0493(2002)130 < 1848:TEVPSI>2.0.CO;2.

Jay, C., B. Marcot, and D. Douglas (2011), Projected status of the Pacific walrus (Odobenus rosmarus divergens) in the twenty-first century, *Polar Biol.*, *34*(7), 1065–1084, doi:10.1007/s00300-011-0967-4.

Johannessen, O., et al. (2004), Arctic climate change: Observed and modelled temperature and sea-ice variability, *Tellus, Ser. A*, *56*(4), 328–341, doi:10.1111/j.1600-0870.2004.00060.x.

Kay, J. E., et al. (2015), The Community Earth System Model (CESM) Large Ensemble Project: A community resource for studying climate change in the presence of internal climate variability, *Bull. Am. Meteorol. Soc.*, *8*, 1333–1349, doi:10.1175/BAMS-D-13-00255.1.

Krishfield, R., J. Toole, A. Proshutinsky, and M. L. Timmermans (2008), Automated ice-tethered profilers for seawater observations under pack ice in all seasons, *J. Atmos. Oceanic Technol.*, *25*(11), 2091–2105, doi:10.1175/2008jtecho587.1.

Large, W. G., J. C. Mcwilliams, and S. C. Doney (1994), Oceanic vertical mixing—A review and a model with a nonlocal boundary-layer parameterization, *Rev. Geophys.*, *32*(4), 363–403, doi:10.1029/94RG01872.

Ledoux, H., and C. Gold (2005), An efficient natural neighbour interpolation algorithm for geoscientific modelling, in *Developments in Spatial Data Handling*, edited by P. F. Fisher, pp. 97–108, Springer, Berlin, doi:10.1007/3-540-26772-7_8.

Lemieux, J.-F., et al. (2015), The Regional Ice Prediction System (RIPS): Verification of forecast sea ice concentration, *Q. J. R. Meteorol. Soc.*, doi:10.1002/qj.2526, in press.

Lipscomb, W. (2001), Remapping the thickness distribution in sea ice models, *J. Geophys. Res.*, *106*(C7), 13,989–14,000, doi:10.1029/2000JC000518.

Markus, T., and D. J. Cavalieri (2000), And enhancement of the NASA Team sea ice algorithm, *IEEE Trans. Geosci. Remote Sens.*, *38*(3), 1387–1398, doi:10.1109/36.843033.

Markus, T., and D. J. Cavalieri (2009), The AMSR-E NT2 sea ice concentration algorithm: Its basis and implementation, *J. Remote Sens. Soc. Jpn.*, *29*(1), 216–225.

Maslowski, W., D. Marble, W. Walczowski, U. Schauer, J. Clement, and A. Semtner (2004), On climatological mass, heat, and salt transports through the Barents Sea and Fram Strait from a pan-Arctic coupled ice-ocean model simulation, *J. Geophys. Res.*, *109*, C03032, doi: 10.1029/2001JC001039.

McGeehan, T., and W. Maslowski (2012), Evaluation and control mechanisms of volume and freshwater export through the Canadian Arctic Archipelago in a high-resolution pan-Arctic ice-ocean model, *J. Geophys. Res.*, *117*, C00D14, doi:10.1029/2011JC007261.

Meier, W., F. Fetterer, J. S. Stewart, and S. Helfrich (2015), How do sea ice concentrations from operational data compare with passive microwave estimates?, *Ann. Glaciol.*, *56*(69), 332–340, doi:10.3189/2015AoG69A694.

Metzger, E., et al. (2014), US Navy operational global ocean and Arctic ice prediction systems, *Oceanography*, *27*(3), 32–43.

Metzger, E. J., H. E. Hurlburt, A. J. Wallcraft, J. F. Shriver, O. M. Smedstad, P. Thoppil, and D. S. Franklin (2008), Validation test report for the Global Ocean Prediction System v3.0 - 1/12° HYCOM/NCODA phase 1. *Tech*. *Rep. NRL/MR/7320-0809148*, Naval Res. Lab., Stennis Space Cent., Hancock, Miss.

Metzger, E. J., A. J. Wallcraft, P. G. Posey, O. M. Smedstad, and D. S. Franklin (2013), The switchover from NOGAPS to NAVGEM 1.1 atmospheric forcing in GOFS and ACNFS. *Tech. Rep. NRL/MR/7320-13-9486*, Naval Res. Lab., Stennis Space Cent., Hancock, Miss.

Metzger, E. J., P. G. Posey, P. G. Thoppil, T. L. Townsend, A. J. Wallcraft. (2015), Validation test report for the Global Ocean Forecast System 3.1-1/12° HYCOM/NCODA/CICE/ISOP *Tech*. *Rep NRL/NR/7320-15-9579*, Naval Res. Lab., Stennis Space Cent., Hancock, Miss.

Murphy, A. H., and E. S. Epstein (1989), Skill scores and correlation-coefficients in model verification, *Mon. Weather Rev.*, *117*(3), 572–581, doi:10.1175/1520-0493(1989)117 < 0572:SSACCI>2.0.CO;2.

NIC (2008), *IMS Daily Northern Hemisphere Snow and Ice Analysis at 1 km, 4 km, and 24 km Resolutions*, Natl. Snow and Ice Data Cent., Boulder, Colo., doi:10.7265/N52R3PMC.

NIMA (2000), Department of Defense World Geodetic System 1984: Its definition and relationships with local geodetic systems. *Tech. Rep. TR8350.2*, National Imagery and Mapping Agency, St. Louis, Mo.

Posey, P. G., E. J. Metzger, A. J. Wallcraft, R. H. Preller, O. M. Smedstad, and M. W. Phelps (2010), Validation of the 1/12° Arctic Cap Nowcast/Forecast System (ACNFS), *Tech. Rep. NRL/MR/7320-10-9287*, Naval Res. Lab., Stennis Space Centre, Mass.

Posey, P. G., E. J. Metzger, A. J. Wallcraft, D. A. Hebert, R. A. Allard, O. M. Smedstad, M. W. Phelps, F. Fetterer, J. S. Stewart, S. R. Helfrich (2015), Improving Arctic sea ice edge forecasts by assimilating high horizontal resolution sea ice concentration data into the U.S. Navy's ice forecast systems, *Cryosphere*, *9*, 1–11, doi:10.5194/tc-9-1-2015.

Preller, R. H., P. G. Posey, W. Maslowski, D. Stark and T. Pham (2002), Navy sea ice prediction systems, *Oceanography*, *15*(1), 44–56.

Rasmussen, T., N. Kliem, and E. Kaas (2010), Modelling the sea ice in the Nares Strait, *Ocean Modell.*, *35*(3), 161–172, doi:10.1016/j.ocemod.2010.07.003.

Sakov, P., F. Counillon, L. Bertino, K. A. Lisæter, P. R. Oke, and A. Korablev (2012), TOPAZ4: An ocean-sea ice data assimilation system for the North Atlantic and Arctic, *Ocean Sci.*, *8*(4), 633–656, doi:10.5194/os-8-633-2012.

Scholz, P., G. Lohmann, Q. Wang, and S. Danilov (2013), Evaluation of a Finite-Element Sea-Ice Ocean Model (FESOM) set-up to study the interannual to decadal variability in the deep-water formation rates, *Ocean Dyn.*, *63*(4), 347–370, doi:10.1007/s10236-012-0590-0.

Schweiger, A., and J. Zhang (2015), Accuracy of short-term sea ice drift forecasts using a coupled ice-ocean model, *J. Geophys. Res. Oceans.*, doi:10.1002/2015JC011273 (accepted, in press).

Schweiger, A., R. Lindsay, J. Zhang, M. Steele, H. Stern, and R. Kwok (2011), Uncertainty in modeled Arctic sea ice volume, *J. Geophys. Res.*, *116*, C00D06, doi:10.1029/2011JC007084.

Serreze, M., M. Holland, and J. Stroeve (2007), Perspectives on the Arctic's shrinking sea-ice cover, *Science*, *315*(5818), 1533–1536, doi: 10.1126/science.1139426.

Serreze, M. C., and J. Stroeve (2015), Arctic sea ice trends, variability, and implications for seasonal ice forecasting. *Philos. Trans. R. Soc. A*, *373*, 1–16, doi:10.1098/rsta.2014.0159.

Smith, G. C., et al. (2015), Sea ice forecast and verification in the Canadian Global Ice Ocean Prediction System, *Q. J. R. Meteorol. Soc.*, doi: 10.1002/qj.2555. (in press).

Snyder, J. P. (1987), Map projections––A working manual, *Tech. Rep. 1395*, U.S. Gov. Print. Off., Washington, D. C., ISBN: 87-ti00250. [Available at http://pubs.usgs.gov/pp/1395/report.pdf, last accessed 2 Oct. 2015.]

Stammer, D., C. Wunsch, R. Giering, C. Eckert, P. Heimbach, J. Marotzke, A. Adcroft, C. Hill, and J. Marshall (2002), Global ocean circulation during 1992-1997, estimated from ocean observations and a general circulation model, *J. Geophys. Res.*, *107*(C9), 3118, doi:10.1029/2001JC000888.

Toole, J. M., R. A. Krishfield, M. L. Timmermans, and A. Proshutinsky (2011), The ice-tethered profiler: ARGO of the Arctic, *Oceanography*, *24*(3), 126–135.

U.S. Navy (2014), *U.S. Navy Arctic Roadmap 2014-2030*, CreateSpace Publishing, Washington, D. C.

van Scheltinga, A., P. Myers, and J. Pietrzak (2010), A finite element sea ice model of the Canadian Arctic Archipelago, *Ocean Dyn.*, *60*(6), 1539–1558, doi:10.1007/s10236-010-0356-5.

Van Woert, M., C. Zou, W. Meier, P. Hovey, R. Preller, and P. Posey (2004), Forecast verification of the Polar Ice Prediction System (PIPS) sea ice concentration fields, *J. Atmos. Oceanic Technol.*, *21*(6), 944–957, doi:10.1175/1520-0426(2004)021 < 0944:FVOTPI>2.0.CO;2.

Wunsch, C., and P. Heimbach (2013), Dynamically and kinematicallly consistent global ocean circulation and ice state estimates. in *Ocean Circulation and Climate: A 21 Century Perspective*. edited by G. Siedler, et al., Intern. Geophys., vol. 103, pp. 553–579, Academic Press, Oxford, U. K.

Zhang, J., and R. Lindsay, A. Schweiger, and I. Rigor (2012), Recent changes in the dynamic properties of declining Arctic Sea Ice: A model study, *Geopohys. Res. Lett.*, *39*, L20503, doi:10.1029/2012GL053545.

Zhang, J., and D. Rothrock (2003), Modeling global sea ice with a thickness and enthalpy distribution model in generalized curvilinear coordinates, *Mon. Weather Rev.*, *131*(5), 845–861, doi:10.1175/1520-0493(2003)131 < 0845:MGSIWA>2.0.CO;2.